

Topologically localized insulators

Bastien Lapiere, Titus Neupert, Luka Trifunovic¹

¹*Department of Physics, University of Zurich, Winterthurerstrasse 190, 8057 Zurich, Switzerland*
(Dated: April 3, 2023)

We show that fully-localized, three-dimensional, time-reversal-symmetry-broken insulators do not belong to a single phase of matter but can realize topologically distinct phases that are labelled by integers. The phase transition occurs only when the system becomes conducting at some filling. We find that these novel topological phases are fundamentally distinct from insulators without disorder: they are guaranteed to host delocalized boundary states giving rise to the quantized boundary Hall conductance, whose value is equal to the bulk topological invariant.

Introduction — The discovery of quantum Hall effect revealed that topology, a branch of mathematics, plays an important role for understanding properties of quantum materials. Topological quantum materials are typically bulk insulators with boundaries that are perfect metals [1, 2]. Further developments [2, 3] showed that superconductors can be topological, too. These developments led to the complete classification of (non-interacting) topological phases, the result known as tenfold-way or “periodic table of topological phases of matter” [4, 5]. The modes that appear on the boundary of topological quantum materials are called topological and anomalous — they typically give rise to either quantized electrical or thermal responses and promise many applications in the areas of quantum computing [3], backscattering-free quantum transport, and even catalysis [6].

More recently [7–15], it was shown that crystalline symmetry adds a new twist to the topological classification: a three-dimensional topological crystalline insulator or superconductor can have topological modes (states) appearing on its hinges (corners) while its faces (and hinges) are insulating. Interestingly [10, 16, 17], crystalline symmetry can turn an atomic insulator topological, in which case they may or may not have fractionally quantized boundary charges. Moreover, the crystalline symmetry facilitates the discovery of topological materials [18–22], with many thousand candidates being predicted [18, 23] and some experimentally confirmed [24–28].

Not only the boundary of a topological material but also its bulk electronic states have intriguing properties: all topological insulators, in the absence of crystalline and sublattice symmetries, have an obstruction to full localization of its occupied bulk electronic states [29]. This property is best studied in the case of quantum Hall insulators [30], where in the presence of disorder topology guarantees the existence of a single energy per Landau level where delocalized states appear. Similarly, the obstruction to full localization was established for the case of quantum spin Hall [31] and three-dimensional topological insulators [32]. Hence, within the tenfold-way paradigm, a fully localized insulator (i.e., an Anderson insulator at all fillings) is guaranteed to be topologically

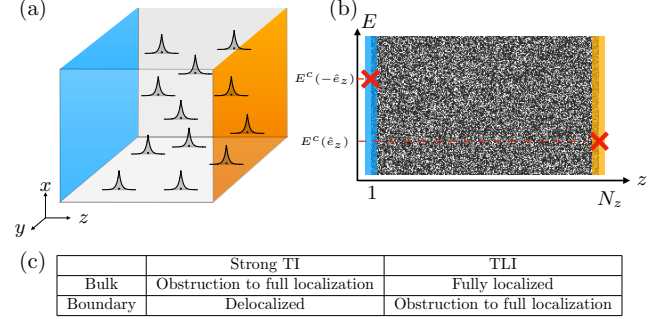


FIG. 1. (a) TLI with $N_{\text{TLI}} = 1$ for open boundary conditions along z -direction only: all the bulk states are localized by disorder, while the two boundary surfaces (orange and blue) host delocalized states and have opposite quantized Hall conductance. (b) The energies $E^c(\pm\hat{e}_z)$ of delocalized states are not constrained by the bulk. (c) Comparison between TLIs and strong TIs. (A TI is called strong if its existence does not rely on translational symmetry.)

trivial.

In this work, we introduce a new notion of topology that applies to fully localized insulators, i.e., Anderson insulator at *all* fillings, in contrast to tenfold-way topological phases which are required to be insulating only at one particular filling [33]. In particular, we consider three-dimensional systems without time-reversal symmetry and find topologically distinct fully localized insulators that can be labelled by integers. The phase transition can occur only if the system becomes conducting at some filling. We refer to these topologically non-trivial phases as *topologically localized insulators* (TLIs). We show that, although all the bulk states of a TLI are exponentially localized, there is an obstruction to localizing them all the way down to an atomic limit. Importantly, electronic states with support close to the boundary carry quantized Hall conductance which can be measured in the Corbino geometry via flux insertion. Note that, for the slab geometry in Fig. 1a, the boundary consists of two disjoint planes with normals $\pm\hat{e}_z$, and the Hall conductances of these two planes are quantized to the opposite value due to their opposite orientation. Furthermore, at each of these planes, topologically protected delocalized

states [30] emerge and remain so under an arbitrarily strong disorder at the boundary, see Fig. 1b–c. We conclude that the boundary of a TLI is anomalous since it cannot be realized as a two-dimensional system: a disordered two-dimensional Chern insulator can host delocalized bulk states only up to disorder strengths that do not close its mobility gap [34]. (A Chern insulator is a locally finite-dimensional Hilbert-space version of Quantum Hall Insulator.)

Model — We construct a TLI by stacking two-dimensional layers in z -direction. We divide the Hilbert space spanned by electronic orbitals of a single layer into the blue and the orange subspaces, see Fig. 2a. We require that for the blue (orange) subspace filled with electrons, the layer has Hall conductance $\sigma_{xy} = e^2/h$ ($\sigma_{xy} = -e^2/h$). Hence, not all blue (orange) orbitals in Fig. 2(a) can be exponentially localized. On the other hand, if we couple the blue orbitals from the layer z to the orange orbitals from the layer $z + 1$, the hybridized orbitals can be all exponentially localized, as in the case of eigenstates of the following tight-binding model of a TLI

$$H = \sum_{\vec{R}\alpha, \vec{R}'\alpha'} t_{\vec{R}\alpha}^{\vec{R}'\alpha'} |\vec{R}\alpha\rangle \langle \vec{R}'\alpha'|, \quad (1)$$

with the hopping amplitudes and onsite potentials (for $\vec{R} = \vec{R}'$) expressed as

$$t_{\vec{R}\alpha}^{\vec{R}'\alpha'} = \sum_{\vec{R}''\alpha''} W_{\vec{R}''\alpha''} C_{\vec{R}\alpha}^{\vec{R}''\alpha''} (C_{\vec{R}'\alpha'}^{\vec{R}''\alpha''})^*. \quad (2)$$

The atomic orbitals of the above stack of layers are denoted by $|\vec{R}\alpha\rangle$, with $\alpha \in \{1, 2\}$ an orbital degree of freedom and \vec{R} a three-dimensional cubic lattice vector. $W_{\vec{R}\alpha}$ are independent, uniformly distributed in $[-W, W]$, random real numbers. The coefficients $C_{\vec{R}'\alpha'}^{\vec{R}\alpha}$ are defined through the lattice vector basis expansion of the wavefunctions

$$|w_{\vec{R}\alpha}\rangle \equiv \mathcal{P}_z^- |\vec{R}\alpha\rangle + \mathcal{P}_{z+1}^+ |(\vec{R} + \hat{e}_z)\alpha\rangle, \quad (3)$$

i.e., $|w_{\vec{R}\alpha}\rangle = \sum_{\vec{R}'\alpha'} C_{\vec{R}'\alpha'}^{\vec{R}\alpha} |\vec{R}'\alpha'\rangle$, where \mathcal{P}_z^+ (\mathcal{P}_z^-) is the projector onto the blue (orange) subspace of the layer z . Such \mathcal{P}_z^+ and \mathcal{P}_z^- can be obtained as the projectors on the occupied and empty bands of a two-band (disorder-free) Chern insulator defined on layer z (see [35] for a concrete model). It is crucial to note that $|w_{\vec{R}\alpha}\rangle$ are exponentially localized, and orthonormal $\langle w_{\vec{R}'\alpha'} | w_{\vec{R}\alpha} \rangle = \delta_{\vec{R}\vec{R}'} \delta_{\alpha\alpha'}$, leading to exponentially decaying matrix elements $t_{\vec{R}\alpha}^{\vec{R}'\alpha'}$, see Fig. 2b. The exponential localization of $|w_{\vec{R}\alpha}\rangle$ follows from that of $\mathcal{P}_z^\pm |\vec{R}\alpha\rangle$ [36], whereas orthonormality can be satisfied only for the Hilbert space onto which $(\mathcal{P}_z^- + \mathcal{P}_{z+1}^+)$ projects, see [35]. The states $|w_{\vec{R}\alpha}\rangle$ form a complete set of localized eigenstates of H under periodic boundary conditions (PBC).

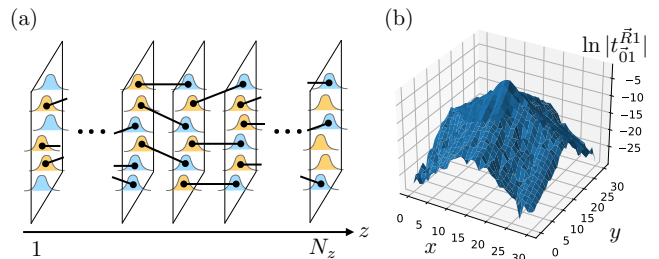


FIG. 2. (a) TLI construction from stack of two-dimensional layers in z -direction. The Hilbert space of each layer is divided into two subspaces spanned by blue and orange orbitals: occupying only blue (orange) orbitals with electrons results in quantized Hall conductance of the layer $\sigma_{12} = e^2/h$ ($\sigma_{12} = -e^2/h$). The blue (orange) orbitals cannot all have exponential localization; Exponential localization is obtained by hybridizing differently colored orbitals from neighbouring layers. (b) Distance dependence of the hopping elements $\ln |t_{01}^{\vec{R}1}|$ of the TLI with $\vec{R} = (x, y, 0)$ for the system size $N_x = N_y = 31$, where $t_{01}^{\vec{R}1}$ is defined below Eq. (1). We observe an exponential decay of the hopping elements $t_{01}^{\vec{R}1}$ in all directions.

From the above construction it is evident that for a z -terminated crystal, there are unpaired blue (orange) orbitals on the layer $z = 1$ ($z = N_z$) which, when filled with electrons, give quantized Hall conductance $\sigma_{xy} = e^2/h$ ($\sigma_{xy} = -e^2/h$), see Fig. 1. Additionally, if a magnetic flux quantum $\Phi_0 = h/e$ is threaded through the layers, the blue subspace of each layer expands to accommodate one more electron while the orange subspace shrinks by the same amount — this statement is known as Streda’s theorem [37]. Hence, if the bulk is fully filled with electrons, the applied flux Φ_0 transfers one electron from layer z to layer $z + 1$ resulting in the bulk polarization $P_z \sim 1$. Accordingly, the corresponding component of the bulk magnetoelectric polarizability tensor is quantized, $(\alpha_{ME})_{zz} = 1$.

The construction presented above resembles pictorially the construction of both one-dimensional dimerized Su-Schrieffer-Heeger model [38] and Kitaev chain [3]; Despite this similarity, we find the obtained phase to be truly three-dimensional: the quantized surface Hall conductance takes the same value for every orientation of the boundary as we demonstrate numerically further below. Furthermore, the bulk magnetoelectric polarizability tensor is found to be isotropic $\alpha_{ME} \equiv (\alpha_{ME})_{ii} = 1$. This statement is further corroborated by the existence of a truly three-dimensional bulk topological invariant.

Bulk topological invariant N_{TLI} — For a bulk Hamiltonian H , with all eigenstates localized, the unitary U that diagonalizes H can be chosen such that its matrix elements are exponentially localized in the basis $|\vec{R}\alpha\rangle$

$$\langle \vec{R}'\alpha' | U | \vec{R}\alpha \rangle \sim e^{-\gamma|\vec{R}-\vec{R}'|}, \quad (4)$$

for some positive constant γ . More concretely, we define U as mapping localized eigenstates $|\psi_n\rangle$ of H onto atomic orbitals $|\vec{R}\alpha\rangle$, i.e., $U|\vec{R}\alpha\rangle = |\psi_{n(\vec{R},\alpha)}\rangle$, such that condition (4) is satisfied. The assignment defined by $n(\vec{R},\alpha)$ is not unique [39]. The bulk integer invariant can be expressed [40] $N_{\text{TLI}} = \nu[U]$,

$$\nu[U] = \frac{i\pi\epsilon^{ijk}}{3V} \text{Tr} \left(U^\dagger [\hat{X}_i, U] U^\dagger [\hat{X}_j, U] U^\dagger [\hat{X}_k, U] \right), \quad (5)$$

with $V = N_x N_y N_z$ being the volume of the system and $\hat{X}_i = \sum_{\vec{R}\alpha} R_i |\vec{R}\alpha\rangle \langle \vec{R}\alpha|$ the i th component of the position operator, $i = 1, 2, 3$, $\vec{R} = (x, y, z)$, and the summation over repeated indices is assumed. The above expression is guaranteed to take integer values as long as (4) is satisfied [41]. Note that for a finite system size, the commutators $[\hat{X}_i, U]$ need to be approximated, see [35]. It can be analytically shown that $N_{\text{TLI}} = 1$ for the model (1), see [35].

Expression for the boundary Hall conductance σ_{12}^∂ — We consider a slab geometry with the width much larger than the localization length. Let us denote the eigenstates of H that are localized on one of the two surfaces by $\{|\psi_n^{\text{surf}}\rangle\}$, irrespective of their energy. Since all the bulk states are localized, some of these states can be safely included in the set $\{|\psi_n^{\text{surf}}\rangle\}$ without affecting the resulting surface Chern number. The Hall conductance of the system when the states $\{|\psi_n^{\text{surf}}\rangle\}$ are filled with electrons is given by the Chern number [34] $\sigma_{12}^\partial = \frac{e^2}{h} \text{Ch}[\mathcal{P}^{\text{surf}}]$,

$$\text{Ch}[\mathcal{P}] = \frac{2\pi i}{N_1 N_2} \text{Tr} \left(\mathcal{P} \left[[\hat{X}_1, \mathcal{P}], [\hat{X}_2, \mathcal{P}] \right] \right), \quad (6)$$

where $\mathcal{P}^{\text{surf}} = \sum_n |\psi_n^{\text{surf}}\rangle \langle \psi_n^{\text{surf}}|$ and $\hat{X}_{1,2}$ are the two components of the position operator along the slab. When the matrix elements of $\mathcal{P}^{\text{surf}}$ are exponentially localized, analogous to condition (4) with $\mathcal{P}^{\text{surf}}$ in place of U , $\text{Ch}[\mathcal{P}^{\text{surf}}]$ is guaranteed to take integer values [34].

The bulk-boundary correspondence of TLIs takes the following form

$$\sigma_{12}^\partial = N_{\text{TLI}} \frac{e^2}{h}. \quad (7)$$

We demonstrated that the above relation holds for the model above Eq. (1), for the z -terminated crystal. Below we demonstrate numerically that it also holds for the x - and y -terminated crystals (hard-wall boundary), as well as for a perturbed version of the model (1). The general proof of relation (7) for an arbitrary model of a TLI in the same phase as (1) directly follows, as the surface Hall conductance can change only if delocalized states move to the surface, which is forbidden for TLIs in the same phase as all the states in the bulk are localized.

The quantized Hall conductance of a TLI's boundary comes together with the quantized (isotropic) magnetoelectric polarizability coefficient α_{ME} of its bulk. This

follows directly from the arguments presented in Ref. 42: when the slab is fully filled with electrons, the electrons are “inert” and do not respond to an external magnetic field. Since the boundary has non-zero quantized Hall conductance, it follows from the Streda theorem [37] that the filling of the boundary changes by an integer amount ($\sigma_{12}^\partial h/e^2$) when the flux $\Phi_0 = h/e$ threads the slab. This charge needs to be compensated by the bulk; From this compensation, it follows that the bulk, fully filled with electrons, has an isotropic and quantized magnetoelectric polarizability tensor $\alpha_{\text{ME}} = N_{\text{TLI}}$. We finally note that an alternative construction of TLI can be found in App. E, based on the Hopf insulator [43]. In particular, the notion of surface Chern number appears in the context of Hopf insulator [44], although in that context, it strongly relies on the translation symmetry.

Numerical results — We perturb the model in Eq. (1) by including nearest-neighbor hopping that eventually push the TLI into a metallic phase. We define $H(\lambda) = H + \lambda H'$ with

$$H' = \sum_{\langle \vec{R}\vec{R}' \rangle_\alpha} \left(t_1 |\vec{R}'\alpha\rangle \langle \vec{R}\alpha| + t_2 |\vec{R}'\alpha\rangle \langle \vec{R}\bar{\alpha}| \right) + \text{h.c.}, \quad (8)$$

where $\bar{1} = 2$, $\bar{2} = 1$, and $\langle \vec{R}, \vec{R}' \rangle$ denotes summation over all nearest-neighbor pairs of lattice vectors. Below, we set $t_1 = 10t_2 = 1$, $W = 1$, and consider one-parameter family of the Hamiltonians $H(\lambda)$, $0 \leq \lambda \leq 1$.

We first study the metal-insulator transition using level spacing statistics. To this end, we compute the average level spacing ratio [45, 46] $r = \langle \langle r_n \rangle_n \rangle_W$ around the middle of the spectrum, where $r_n = \min\{s_n, s_{n+1}\} / \max\{s_n, s_{n+1}\}$ with $s_n = E_{n+1} - E_n \geq 0$ being the level spacing and E_n , $n = 1, \dots, 2V$, the ordered eigenvalues of $H(\lambda)$. For $\lambda < \lambda_c$, r decreases with increasing system size, approaching the value $r_{\text{PE}} \approx 0.38$ of the Poisson Ensemble (PE). All eigenstates are localized in this regime. For $\lambda > \lambda_c$, r increases with increasing system size, approaching the value $r_{\text{GUE}} \approx 0.60$ of the Gaussian Unitary Ensemble (GUE). The system is in a metallic phase at half-filling (a mobility edge appears). From this one-parameter scaling, we find the metal-insulator transition at half-filling occurs at $\lambda_c \approx 0.088 \pm 0.002$, see Fig. 3a.

As long as $H(\lambda)$ is in the localized phase, the condition (4) is satisfied and N_{TLI} and σ_{12}^∂ are guaranteed to take integer values for large enough system size [34, 41]. In practice, for the system sizes we consider in Fig. 3, we find that the quantization of N_{TLI} and $\sigma_{12}^\partial h/e^2$ breaks before the value of λ_c is reached. In Fig. 3, we show that the range of λ for which N_{TLI} and $\sigma_{12}^\partial h/e^2$ are quantized extends as the system size is increased, showing the tendency towards the value λ_c .

We note that although the tight-binding model (1) has exponentially decaying hopping amplitudes (Fig. 2), the system remains in the same phase for a finite-range hop-

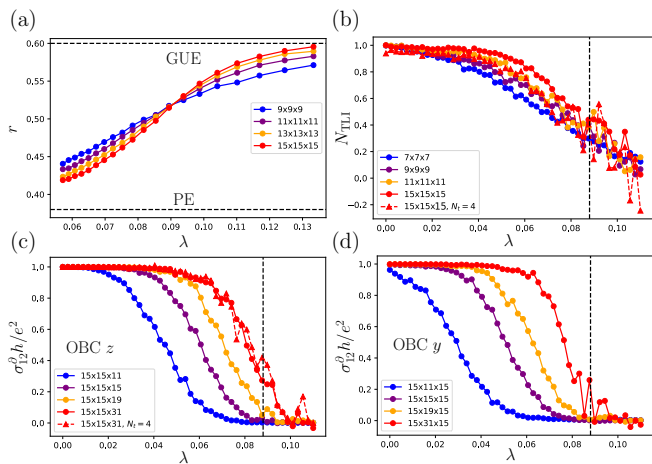


FIG. 3. (a) Estimate of λ_c from mean level spacing ratio r as function of λ . r is computed over 500 eigenstates in the middle of the spectrum, considering 10^3 disorder realizations. (b) The winding number N_{TLI} is computed for different system sizes with increasing hopping strength λ , where the quantized plateau increases with system size for $\lambda < \lambda_c$. (c) Surface Chern number for the hard-wall termination in z -direction as function of λ . (d) Same as (c), for the termination in y -direction. No disorder averaging was performed for the winding and Chern numbers, apart from the blue curves where average was performed over 5 disorder realizations as well as the red curves in (b) and (c) for $\lambda < \lambda_c$. The dashed curves in panels c-d are for the finite-range hopping version of the model (1) with $N_t = 4$, see the main text.

ping version of this model. We have checked this explicitly by truncating the exponential tail of the wavefunctions $|w_{\vec{R}\alpha}\rangle$, i.e., setting $C_{\vec{R}'\alpha'}^{\vec{R}\alpha} = 0$ for $|\vec{R} - \vec{R}'| > N_t$. The results for $N_t = 4$ are given by dashed curves in Fig. 3c–d, from where one can conclude that the phase is stable under such truncation, although the truncation increases the localization length as indicated by less good quantization.

Quantized Hall response — The quantized response of a TLI can be probed in the Corbino geometry by adiabatic flux insertion. Since the TLI’s bulk is fully localized, the boundary can be doped with electrons independently of the bulk. The boundary of a TLI, fully filled with electrons, gives the same response to flux insertion as a torus-shaped, half-filled two-dimensional Chern insulator (extrinsic second-order TI [47]), see [35]. The main difference between these two setups is that the response of a TLI remains quantized under an arbitrarily strong boundary disorder, whereas a half-filled Chern insulator gets trivialized above certain critical disorder strength [34].

Resonant energy model for a TLI — In the model defined in Eq. (1) disorder is introduced in a highly nontrivial way that is not natural to occur in experimental systems. Here we suggest an alternative model realization of a TLI can be obtained by stacking two-dimensional

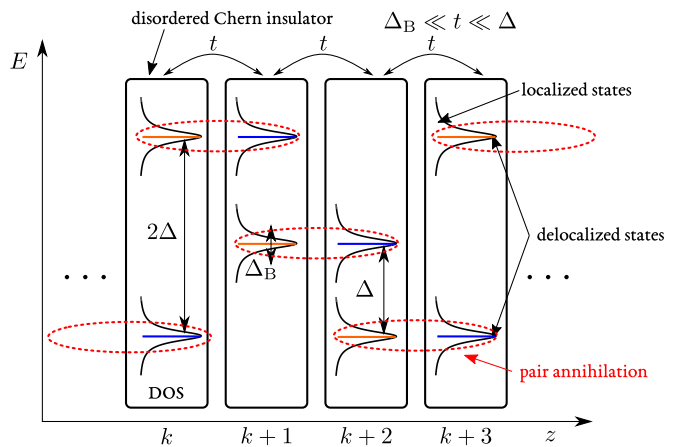


FIG. 4. Sketch of the layer construction for the three-dimensional TLI. A stack along z -direction of two-band disordered Chern insulators, with the bandwidth Δ_B and the gap Δ or 2Δ , becomes fully localized due to interlayer coupling t such that $\Delta_B \ll t \ll \Delta$. For each layer, density of states (DOS) is shown, and the delocalized states depicted in orange (blue) carry a positive (negative) quantized Hall conductance.

Chern insulators with generic disorder. We assume that each Chern insulator has two bands and a band gap Δ or 2Δ (depending on the layer) that is much larger than the band width. Disorder will broaden the “bands” to a band with Δ_b , but should be weak enough to maintain $\Delta_b \ll \Delta$. There is a single energy per band [34] where delocalized states appear. We mark these energies in blue or orange in Fig. 4, depending on the sign of their quantized Hall conductance. The parameters of the layers repeat with the period three, and the system is tuned such that differently colored delocalized states from neighbouring layers are on-resonance. When only resonant interlayer coupling is considered, the model is dimerized, with each dimer being a fully localized phase since it belongs to a two-dimensional unitary class and has zero Hall conductance. Hence, the delocalized states from neighbouring layers “pair annihilate”, leaving only unpaired delocalized states on the boundary of the resulting three-dimensional system. We anticipate the localization length (in the xy -plane) of each dimer to be rather large in this model due to exponential sensitivity of the localization length in two-dimensional unitary class [48]. The off-resonant interlayer coupling tends to delocalize some bulk states, but we expect for strong enough disorder and for large enough flatness ratio Δ/Δ_B (see Fig. 4) that the system is in the same phase as the above-mentioned dimerized limit. The detailed study of the model is left for the future works.

Conclusions — Topology of tenfold-way (strong) TIs [2, 4, 5] poses an obstruction to localization by disorder of its occupied bulk states [30–32]. Correspondingly, Topological Anderson Insulators [49] are Anderson insulators only at certain but not all fillings and the topo-

logical charge is carried by their delocalized bulk states only. Our main result is finding that fully-localized insulators can be topologically non-trivial, too. In particular, we construct a three-dimensional model with broken time-reversal symmetry, where topology poses an obstruction to localization of its fully-localized bulk states all the way down to the atomic limit. We find that the three-dimensional fully-localized insulator, with broken time-reversal symmetry, does not represent a single phase of matter, but rather contains infinitely many phases that are labeled by integers. Here, the Anderson model of localization, in the absence of mobility edge, corresponds to topologically trivial insulator and is labelled by $N_{\text{TLLI}} = 0$, whereas topologically non-trivial localized insulators are guaranteed to host states delocalized along the crystal's insulating boundary that give rise to the quantized Hall conductance (7) in Corbino geometry. Crucially, these delocalized boundary states remain topologically protected in the presence of an arbitrarily strong boundary disorder. We introduced the method to construct these novel insulators, which is readily generalizable to include additional symmetries (e.g. time-reversal). We hope that this work will motivate experiments where quantized responses are observed in out-of-equilibrium settings.

Acknowledgments — The authors acknowledge stimulating discussions with Ö. M. Aksoy, P. W. Brouwer, A. Furusaki, and C. Mudry. We are thankful to P. W. Brouwer for pointing up similarities between TLLIs and extrinsic higher-order TIs. BL acknowledges funding from the European Research Council (ERC) under the European Union's Horizon 2020 research and innovation program (ERC-StG-Neupert-757867-PARATOP). LT acknowledges financial support from the FNS/SNF Ambizione Grant No. PZ00P2_179962.

-
- [1] S. Ryu, C. Mudry, H. Obuse, and A. Furusaki, Phys. Rev. Lett. **99**, 116601 (2007).
- [2] A. P. Schnyder, S. Ryu, A. Furusaki, and A. W. W. Ludwig, Phys. Rev. B **78**, 195125 (2008).
- [3] A. Y. Kitaev, Phys. Usp. **44**, 131 (2001).
- [4] A. Kitaev, AIP Conference Proceedings **1134**, 22 (2009).
- [5] A. P. Schnyder, S. Ryu, A. Furusaki, and A. W. W. Ludwig, AIP Conference Proceedings **1134**, 10 (2009).
- [6] J. Chen, X. Y. He, K. H. Wu, Z. Q. Ji, L. Lu, J. R. Shi, J. H. Smet, and Y. Q. Li, Phys. Rev. B **83**, 241304 (2011).
- [7] F. Schindler, A. M. Cook, M. G. Vergniory, Z. Wang, S. S. P. Parkin, B. A. Bernevig, and T. Neupert, Science Advances **4** (2018), 10.1126/sciadv.aat0346.
- [8] Z. Song, Z. Fang, and C. Fang, Phys. Rev. Lett. **119**, 246402 (2017).
- [9] J. Langbehn, Y. Peng, L. Trifunovic, F. von Oppen, and P. W. Brouwer, Phys. Rev. Lett. **119**, 246401 (2017).
- [10] L. Trifunovic, Phys. Rev. Research **2**, 043012 (2020).
- [11] T. Papenbrock, L. Kaplan, and G. F. Bertsch, Phys. Rev. B **65**, 235120 (2002).
- [12] S. A. A. Ghorashi, T. Li, and T. L. Hughes, Phys. Rev. Lett. **125**, 266804 (2020).
- [13] A. K. Ghosh, T. Nag, and A. Saha, Phys. Rev. B **104**, 134508 (2021).
- [14] T. Nag, V. Juričić, and B. Roy, Phys. Rev. B **103**, 115308 (2021).
- [15] Y.-B. Yang, K. Li, L.-M. Duan, and Y. Xu, Phys. Rev. B **103**, 085408 (2021).
- [16] W. A. Benalcazar, B. A. Bernevig, and T. L. Hughes, Phys. Rev. B **96**, 245115 (2017).
- [17] H. Watanabe and H. C. Po, Phys. Rev. X **11**, 041064 (2021).
- [18] B. Bradlyn, L. Elcoro, J. Cano, M. G. Vergniory, Z. Wang, C. Felser, M. I. Aroyo, and B. A. Bernevig, Nature **547**, 298 (2017).
- [19] H. C. Po, A. Vishwanath, and H. Watanabe, Nature Comm. **8**, 50 (2017).
- [20] M. Geier, P. W. Brouwer, and L. Trifunovic, Phys. Rev. B **101**, 245128 (2020).
- [21] A. Skurativska, T. Neupert, and M. H. Fischer, Phys. Rev. Research **2**, 013064 (2020).
- [22] S. Ono, L. Trifunovic, and H. Watanabe, Phys. Rev. B **100**, 245133 (2019).
- [23] T. Zhang, Y. Jiang, Z. Song, H. Huang, Y. He, Z. Fang, H. Weng, and C. Fang, Nature **566**, 475 (2019).
- [24] M. König, S. Wiedmann, C. Brüne, A. Roth, H. Buhmann, L. W. Molenkamp, X.-L. Qi, and S.-C. Zhang, Science **318**, 766 (2007).
- [25] S. Wu, V. Fatemi, Q. D. Gibson, K. Watanabe, T. Taniguchi, R. J. Cava, and P. Jarillo-Herrero, Science **359**, 76 (2018).
- [26] Y. Xia, D. Qian, D. Hsieh, L. Wray, A. Pal, H. Lin, A. Bansil, D. Grauer, Y. S. Hor, R. J. Cava, and M. Z. Hasan, Nature Phys. **5**, 398 (2009).
- [27] S. Ran, C. Eckberg, Q.-P. Ding, Y. Furukawa, T. Metz, S. R. Saha, I.-L. Liu, M. Zic, H. Kim, J. Paglione, and N. P. Butch, Science **365**, 684 (2019).
- [28] A. Murani, A. Kasumov, S. Sengupta, Y. A. Kasumov, V. T. Volkov, I. I. Khodos, F. Brisset, R. Delagrè, A. Chepelianskii, R. Deblock, H. Bouchiat, and S. Guéron, Nature Communications **8**, 15941 (2017).
- [29] A similar statement in case of topological band insulators in the absence of crystalline and sublattice symmetries: there is an obstruction to spanning the Hilbert space of occupied electronic states by exponentially localized or compact Wannier functions [50].
- [30] J. T. Chalker and P. D. Coddington, Journal of Physics C: Solid State Physics **21**, 2665 (1988).
- [31] M. Onoda, Y. Avishai, and N. Nagaosa, Phys. Rev. Lett. **98**, 076802 (2007).
- [32] T. Morimoto, A. Furusaki, and C. Mudry, Phys. Rev. B **91**, 235111 (2015).
- [33] Topological Anderson Insulators [49], that are captured by tenfold-way classification [2, 3], have delocalized states in the bulk and hence do not represent fully localized insulators.
- [34] E. Prodan, Journal of Physics A: Mathematical and Theoretical **44**, 113001 (2011).
- [35] “See supplementary material.”
- [36] T. Thonhauser and D. Vanderbilt, Phys. Rev. B **74**, 235111 (2006).
- [37] P. Streda, Journal of Physics C: Solid State Physics **15**,

- L717 (1982).
- [38] W. P. Su, J. R. Schrieffer, and A. J. Heeger, *Phys. Rev. Lett.* **42**, 1698 (1979).
 - [39] $U(1)$ gauge freedom and non-uniqueness of $n(\vec{R}, \alpha)$ do not affect the value of the bulk invariant.
 - [40] We note that similar invariant appears in the anomalous Floquet-Anderson insulator [51] and its multi-drive generalization [52].
 - [41] J. Song and E. Prodan, *Phys. Rev. B* **89**, 224203 (2014).
 - [42] B. Lapierre, T. Neupert, and L. Trifunovic, *Phys. Rev. Research* **3**, 033045 (2021).
 - [43] J. E. Moore, Y. Ran, and X.-G. Wen, *Phys. Rev. Lett.* **101**, 186805 (2008).
 - [44] A. Alexandradinata, A. Nelson, and A. A. Soluyanov, *Phys. Rev. B* **103**, 045107 (2021).
 - [45] V. Oganesyan and D. A. Huse, *Phys. Rev. B* **75**, 155111 (2007).
 - [46] J. Šuntajs, T. Prosen, and L. Vidmar, *Annals of Physics* , 168469 (2021).
 - [47] M. Geier, L. Trifunovic, M. Hoskam, and P. W. Brouwer, *Phys. Rev. B* **97**, 205135 (2018).
 - [48] A. Furusaki, *Phys. Rev. Lett.* **82**, 604 (1999).
 - [49] J. Li, R.-L. Chu, J. K. Jain, and S.-Q. Shen, *Phys. Rev. Lett.* **102**, 136806 (2009).
 - [50] N. Read, *Phys. Rev. B* **95**, 115309 (2017).
 - [51] P. Titum, E. Berg, M. S. Rudner, G. Refael, and N. H. Lindner, *Phys. Rev. X* **6**, 021013 (2016).
 - [52] D. M. Long, P. J. D. Crowley, and A. Chandran, *Phys. Rev. Lett.* **126**, 106805 (2021).
 - [53] S. Ryu, A. P. Schnyder, A. Furusaki, and A. W. W. Ludwig, *New Journal of Physics* **12**, 065010 (2010).
 - [54] A. Kundu, M. Rudner, E. Berg, and N. H. Lindner, *Phys. Rev. B* **101**, 041403 (2020).

SUPPLEMENTARY MATERIAL

A. Computation of the winding number for the model of TLI

In this section we show that the third winding number for the model (1) is quantized to a non-zero value given by the Chern number of the blue subspace of a single layer (see Fig. 2a of the main text). Although the model (1) lacks translational symmetry, its eigenstates $|w_{\vec{R}\alpha}\rangle$ are related to each other by translational symmetry. Below, we first prove the following relation for the unitary $U = \bigoplus_{\vec{k}} U_{\vec{k}}$ that diagonalizes the model (1)

$$U_{\vec{k}} = \mathcal{U}_{k_x k_y} \mathcal{D} \mathcal{U}_{k_x k_y}^\dagger, \quad (\text{S1})$$

where $\mathcal{U}_{k_x k_y}$ is a unitary that diagonalizes the Bloch Hamiltonian of the two-dimensional, two-band Chern insulator whose positive (negative) energy states define the blue (orange) subspace in Fig. (2a) of the main text; The matrix $\mathcal{D} = \text{diag}(e^{ik_z}, 1)$ translates the Bloch eigenstate with the positive energy by one unit cell in z -direction. The Bloch states with negative energy at layer z , and positive energy at layer $z + 1$ are

$$\begin{cases} |u_{zk_x k_y}^- \rangle = a_{k_x k_y} |z1\rangle + b_{k_x k_y} |z2\rangle, \\ |u_{(z+1)k_x k_y}^+ \rangle = b_{k_x k_y}^* |(z+1)1\rangle - a_{k_x k_y}^* |(z+1)2\rangle, \end{cases} \quad (\text{S2})$$

where we used the notation $\mathcal{U}_{k_x k_y} = \begin{pmatrix} a_{k_x k_y} & b_{k_x k_y}^* \\ b_{k_x k_y} & -a_{k_x k_y}^* \end{pmatrix}$. The two states above are discontinuous over the BZ. We consider linear combination of the two states that is continuous

$$\begin{cases} |\tilde{u}_{k_x k_y}^- \rangle = a_{k_x k_y}^* |u_{zk_x k_y}^- \rangle + b_{k_x k_y} |u_{(z+1)k_x k_y}^+ \rangle, \\ |\tilde{u}_{k_x k_y}^+ \rangle = b_{k_x k_y}^* |u_{zk_x k_y}^- \rangle - a_{k_x k_y} |u_{(z+1)k_x k_y}^+ \rangle. \end{cases} \quad (\text{S3})$$

After performing the Fourier transform in the z -direction, we conclude that the continuous unitary is of the form (S1). In order to compute the third winding of the above unitary, we use Eq. (S9) which gives eight different terms. We can group four of them as

$$2i \text{Tr} \left(\text{diag}(1, 0) \left[\mathcal{U}_{k_x k_y}^\dagger (\partial_{k_x} \mathcal{U}_{k_x k_y}), \mathcal{U}_{k_x k_y}^\dagger (\partial_{k_y} \mathcal{U}_{k_x k_y}) \right] \right) = 2i \left[\mathcal{U}_{k_x k_y}^\dagger (\partial_{k_x} \mathcal{U}_{k_x k_y}), \mathcal{U}_{k_x k_y}^\dagger (\partial_{k_y} \mathcal{U}_{k_x k_y}) \right]_{00}, \quad (\text{S4})$$

additional two terms as

$$ie^{-ik_z} \left((\partial_{k_x} \mathcal{U}_{k_x k_y}^\dagger) \mathcal{U}_{k_x k_y} \mathcal{D} \mathcal{U}_{k_x k_y}^\dagger (\partial_{k_y} \mathcal{U}_{k_x k_y}) - \mathcal{U}_{k_x k_y}^\dagger (\partial_{k_y} \mathcal{U}_{k_x k_y}) \mathcal{D} (\partial_{k_x} \mathcal{U}_{k_x k_y}^\dagger) \mathcal{U}_{k_x k_y} \right)_{00}, \quad (\text{S5})$$

and the two last terms are

$$ie^{ik_z} \left((\partial_{k_x} \mathcal{U}_{k_x k_y}^\dagger) \mathcal{U}_{k_x k_y} \mathcal{D}^* \mathcal{U}_{k_x k_y}^\dagger (\partial_{k_y} \mathcal{U}_{k_x k_y}) - \mathcal{U}_{k_x k_y}^\dagger (\partial_{k_y} \mathcal{U}_{k_x k_y}) \mathcal{D}^* (\partial_{k_x} \mathcal{U}_{k_x k_y}^\dagger) \mathcal{U}_{k_x k_y} \right)_{00}. \quad (\text{S6})$$

The terms (S4)-(S5) cancel out after integrating over k_z from 0 to 2π . Hence, we consider only the terms in Eq. (S4). Using the fact that the Chern number for the lower band reads

$$\text{Ch} = \int_{\text{BZ}} \frac{d^2 k}{2\pi i} \left(\langle \partial_{k_x} u_{k_x, k_y}^- | \partial_{k_y} | u_{k_x, k_y}^- \rangle - \langle \partial_{k_y} u_{k_x, k_y}^- | \partial_{k_x} | u_{k_x, k_y}^- \rangle \right) \quad (\text{S7})$$

together with $\mathcal{U}_{k_x k_y} |0\rangle = |u_{k_x k_y}^- \rangle$, and $\mathcal{U}_{k_x k_y}^\dagger (\partial_{k_x} \mathcal{U}_{k_x k_y}) \mathcal{U}_{k_x k_y}^\dagger (\partial_{k_y} \mathcal{U}_{k_x k_y}) = -(\partial_{k_x} \mathcal{U}_{k_x k_y}^\dagger) (\partial_{k_y} \mathcal{U}_{k_x k_y})$, we obtain

$$\nu[U_{\vec{k}}] = \text{Ch}. \quad (\text{S8})$$

We note that in the case where $\mathcal{D} = \text{diag}(e^{ilk_z}, 1)$ with $l \in \mathbb{Z}$, the obtained relation becomes $\nu[U_{\vec{k}}] = l\text{Ch}$.

B. Third winding and Chern numbers

For translationally invariant unitaries $U = \bigoplus_{\vec{k}} U_{\vec{k}}$, in the thermodynamic limit, the third winding number is defined

$$\nu[U_{\vec{k}}] = \int_{\text{BZ}} \frac{d^3k}{8\pi^2} \text{Tr} \left(U_{\vec{k}}^\dagger \partial_{k_x} U_{\vec{k}} \left[U_{\vec{k}}^\dagger \partial_{k_y} U_{\vec{k}}, U_{\vec{k}}^\dagger \partial_{k_z} U_{\vec{k}} \right] \right), \quad (\text{S9})$$

while for finite systems, the integral is replaced by a sum over discrete momenta \vec{k} . For unitaries that lack translational symmetry but satisfy condition (4), the third winding number can be defined [41]

$$\nu[U] = \frac{i\pi}{3} \frac{1}{N_x N_y N_z} \epsilon^{ijk} \text{Tr} \left(U^{-1} [\hat{X}_i, U] U^{-1} [\hat{X}_j, U] U^{-1} [\hat{X}_k, U] \right), \quad (\text{S10})$$

where $\hat{X}_i = \sum_{\vec{R}\alpha} R_i |\vec{R}\alpha\rangle \langle \vec{R}\alpha|$ is the position operator in direction $i = 1, 2, 3$, $\vec{R} = (x, y, z)$, and summation over repeated indices is assumed. The above expression takes non-zero integer values only in the thermodynamic limit. In order to apply it to finite systems, we approximate the commutators $[X_i, U]$ by $[\hat{X}_i, U]$, i.e., linear combination of unitaries with integer number of flux quanta inserted

$$[\hat{X}_i, U] = \sum_{m=1}^{N_i-1} c_m e^{2\pi i m \hat{X}_i / N_i} U e^{-2\pi i m \hat{X}_i / N_i}. \quad (\text{S11})$$

The choice of coefficients c_m , giving the correct thermodynamic-limit value of $[X_i, U]$, is not unique [34, 41]. In general, these are the coefficients of the discrete Fourier transform of a function $f(x)$ defined on the circle $[-\lfloor \frac{N_i}{2} \rfloor, \lfloor \frac{N_i}{2} \rfloor]$ that is periodic and equal to $f(x) = x$ for $x < \alpha \lesssim \lfloor \frac{N_i}{2} \rfloor$. In this work, we take c_m to be the Fourier coefficients of the function $f(x) = x$,

$$c_m = \frac{e^{2\pi i m (\lfloor \frac{N_i}{2} \rfloor + 1) / N_i}}{1 - e^{2\pi i m / N_i}}. \quad (\text{S12})$$

Similarly, for a translationally invariant projector $\mathcal{P} = \bigoplus_{k_x k_y} \mathcal{P}_{k_x k_y}$, in the thermodynamic limit, the Chern number of the Hilbert space, onto which this projector projects, is defined [53]

$$\text{Ch}[\mathcal{P}_{k_x k_y}] = i \int_{\text{BZ}} \frac{dk_x dk_y}{2\pi} \text{Tr} \left(\mathcal{P}_{k_x k_y} \left[\partial_{k_x} \mathcal{P}_{k_x k_y}, \partial_{k_y} \mathcal{P}_{k_x k_y} \right] \right), \quad (\text{S13})$$

for finite systems, the above integral is replaced by a sum over discrete momenta (k_x, k_y) . When the projector \mathcal{P} lacks translational symmetry, but satisfied the condition

$$\langle \vec{R}'\alpha' | \mathcal{P} | \vec{R}\alpha \rangle \sim e^{-\gamma |\vec{R} - \vec{R}'|}, \quad (\text{S14})$$

for some positive γ , the Chern number in xy plane in the thermodynamic limit can be defined [34]

$$\text{Ch}[\mathcal{P}] = \frac{2\pi i}{N_x N_y} \text{Tr} \left(\mathcal{P} \left[[\hat{X}_1, \mathcal{P}], [\hat{X}_2, \mathcal{P}] \right] \right). \quad (\text{S15})$$

For finite systems, the commutator $[\hat{X}_1, \mathcal{P}]$ is approximated by $[\hat{X}_1, P]$, see Eq. (S11).

C. Details on numerical calculations

For the numerical calculations in this work, the projectors \mathcal{P}_z^\pm used for the model (1) are obtained as the projectors onto one of the two bands of the following model for Chern insulator

$$H_{2D} = \sin(k_x) \sigma_x + \sin(k_y) \sigma_y + (1 - \cos(k_x) - \cos(k_y)) \sigma_z. \quad (\text{S16})$$

As explained in the main text, the eigenstates of the Hamiltonian (1), are

$$|w_{\vec{R}\alpha}\rangle = (\mathcal{P}_z^- + \mathcal{P}_{z+1}^+) (|\vec{R}\alpha\rangle + |(\vec{R} + \hat{e}_z)\alpha\rangle), \quad (\text{S17})$$

with eigenenergy $W_{\vec{R}\alpha}$. Hence,

$$H = \sum_{\vec{R}\alpha} W_{\vec{R},\alpha} |w_{\vec{R}\alpha}\rangle \langle w_{\vec{R}\alpha}| \quad (\text{S18})$$

In other words, the above Hamiltonian $H = UH_W U^\dagger$ is unitarily related to Hamiltonian H_W of a trivial localized insulator, with the unitary U satisfying the localization condition (4). To show the orthonormality relation $\langle w_{\vec{R}'\alpha'} | w_{\vec{R}\alpha} \rangle = \delta_{\vec{R}\vec{R}'} \delta_{\alpha\alpha'}$, we denote $\vec{R} = (\vec{r}, z)$, with \vec{r} two-dimensional lattice vector, and consider the scalar product

$$\begin{aligned} \langle w_{\vec{r}'z\alpha'} | w_{\vec{r}z\alpha} \rangle &= (\langle \vec{r}'z\alpha' | + \langle \vec{r}'(z+1)\alpha' |) (\mathcal{P}_z^+ + \mathcal{P}_{z+1}^-) (|\vec{r}z\alpha\rangle + |\vec{r}(z+1)\alpha\rangle) \\ &= \langle \vec{r}'z\alpha' | \mathcal{P}_z^+ |\vec{r}z\alpha\rangle + \langle \vec{r}'z\alpha' | \mathcal{P}_z^- |\vec{r}z\alpha\rangle = \delta_{\vec{r}\vec{r}'} \delta_{\alpha\alpha'}, \end{aligned} \quad (\text{S19})$$

where we used that $\mathcal{P}_z^+ + \mathcal{P}_z^- = \mathbb{I}$ on the subspace of the Hilbert space corresponding to the layer z . For $z \neq z'$, it is sufficient to consider $z' = z + 1$,

$$\begin{aligned} \langle w_{\vec{r}(z+1)\alpha} | w_{\vec{r}z\alpha} \rangle &= (\langle \vec{r}(z+1)\alpha | + \langle \vec{r}(z+2)\alpha |) (\mathcal{P}_{z+1}^+ + \mathcal{P}_{z+2}^-) (\mathcal{P}_z^+ + \mathcal{P}_{z+1}^-) (|\vec{r}z\alpha\rangle + |\vec{r}(z+1)\alpha\rangle) \\ &= \langle \vec{r}(z+1)\alpha | \mathcal{P}_{z+1}^+ \mathcal{P}_{z+1}^- |\vec{r}(z+1)\alpha\rangle = 0. \end{aligned} \quad (\text{S20})$$

In the above derivation, we used that $\mathcal{P}_{z+1}^+ \mathcal{P}_{z+1}^- = 0$.

Below, we explain how the unitary U_W of the perturbed model $H(\lambda)$ is constructed

$$H(\lambda) = \sum_{\vec{R}\alpha} \left[W_{\vec{R},\alpha} |w_{\vec{R}\alpha}\rangle \langle w_{\vec{R}\alpha}| + \lambda \sum_{i=1}^3 \left(t_1 \left[|\vec{R} + \hat{e}_i, \alpha\rangle \langle \vec{R}, \alpha | + \text{h.c.} \right] + t_2 \left[|\vec{R} + \hat{e}_i, \alpha\rangle \langle \vec{R}, \bar{\alpha} | + \text{h.c.} \right] \right) \right], \quad (\text{S21})$$

where we set $t_1 = 10t_2 = 1$. All $2V$ eigenstates $\{|\psi_n\rangle\}$ of $H(\lambda)$ are localized for $\lambda < \lambda_c$ in the thermodynamic limit. The unitary U_W is constructed from these localized eigenstates, after sorting them such that U_W maps $|\vec{R}\alpha\rangle$ to the two eigenstates $|\psi_{n(\vec{R},\alpha)}\rangle$, localized closest to the orbitals at $|\vec{R}\alpha\rangle$. To this end, we compute $\arg(\langle \psi_n | e^{2\pi i \hat{X}_j / N_j} | \psi_n \rangle)$, where the operators $e^{2\pi i \hat{X}_j / N_j}$ are compatible with PBC. This way, we obtain the following coordinate vectors on the 3-torus (\mathbb{T}^3)

$$\vec{v}(|\psi_n\rangle) = \left(\frac{N_x}{2\pi} \arg(\langle \psi_n | e^{2\pi i \hat{X} / N_x} | \psi_n \rangle), \frac{N_y}{2\pi} \arg(\langle \psi_n | e^{2\pi i \hat{Y} / N_y} | \psi_n \rangle), \frac{N_z}{2\pi} \arg(\langle \psi_n | e^{2\pi i \hat{Z} / N_z} | \psi_n \rangle) \right)^T, \quad (\text{S22})$$

where we choose the branch cut of $\arg(\xi)$ to be $[0, \infty)$, such that $0 \leq \arg(\xi) < 2\pi$. The sorting procedure is the following: we first minimize the distance between $\vec{v}(|\psi_n\rangle)$ and $\vec{v}(|\vec{R}\alpha\rangle)$ by computing

$$\|\vec{v}(|\vec{R}\alpha\rangle) - \vec{v}(|\psi_n\rangle)\|_{\mathbb{T}^3} = \sqrt{\sum_{i=1}^3 d(R_i, (\vec{v}(|\psi_n\rangle))_i)^2} \quad (\text{S23})$$

where $d(x, y)$ is the following metric on the circle of radius $\frac{N_i}{2\pi}$,

$$d(x, y) = \min\{|x - y|, N_i - |x - y|\}. \quad (\text{S24})$$

To each orbital $|\vec{R}\alpha\rangle$, we associate eigenvector $|\psi_n\rangle$ closest to it according to the metric (S23), unless this eigenvector is already assigned to a different lattice vector, in which case next-closest unassigned eigenvector is used. This defines a unitary U_W , $U_W |\vec{R}\alpha\rangle = |\psi_{n(\vec{R},\alpha)}\rangle$, satisfying the localization condition (4). As the metallic phase is approached, the eigenstates $|\psi_n\rangle$ become plane-wave-like, implying that $|\langle \psi_n | e^{2\pi i \hat{X}_j / N_j} | \psi_n \rangle| \rightarrow 0$. Since $\arg(\xi)$ is not well-defined at $\xi = 0$, the above procedure is not well-define in a metallic phase. For finite systems, we compute $\langle \|\vec{v}(|\psi_n\rangle)\|_{\mathbb{T}^3} \rangle_n$, in order to define the region in parameter space in which the winding number is still well-defined. Such region exists for certain values of λ which are smaller than λ_c , see Fig. 5a.

We now define the projector $\mathcal{P}_W^{\text{surf}}$ onto the surface perpendicular to z -axis. This is achieved by removing localized eigenstates $|\psi_n\rangle$ within the bulk of the system, such that the obtained projector projects onto two decoupled surfaces. We first define the set of localized eigenstates in the bulk of the slab as

$$\text{bulk}(W) = \left\{ |\psi_n\rangle, 1 - \sum_{\substack{x,y,\alpha \\ z=[N_z/2]-L \\ z=[N_z/2]+L}} |\langle \vec{R}\alpha | \psi_n \rangle|^2 < \epsilon \right\}, \quad (\text{S25})$$

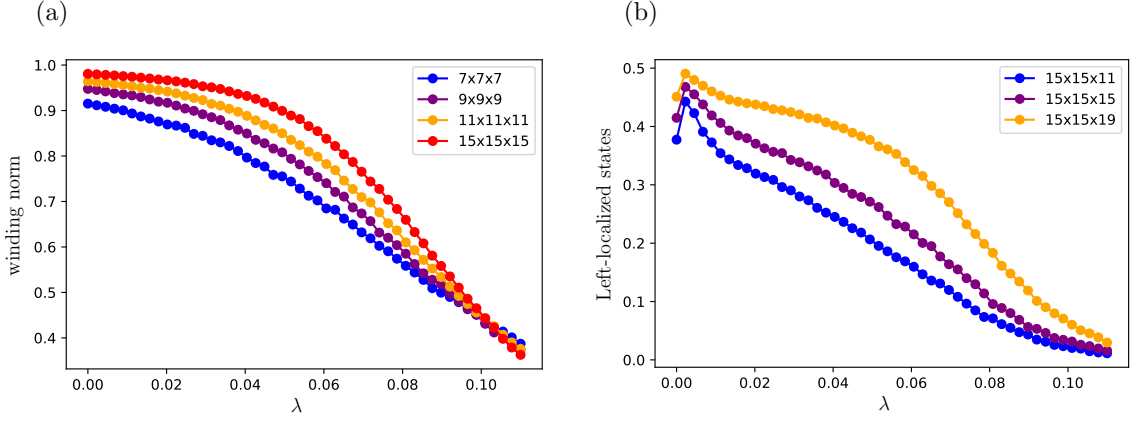


FIG. 5. (a) The average $\langle ||\vec{v}(|\psi_n\rangle)||_{\mathbb{T}^3} \rangle_n$ over all eigenstates as function of parameter λ , see Eq. (S21). This quantity goes from 1, deep in the localized phase, to 0 in the metallic phase. (b) Portion of eigenstates that are localized in the left-half of the system, i.e. for $z \in \{1, \dots, \lfloor N_z/2 \rfloor\}$. This fraction goes from approximately one-half, at $\lambda = 0$, to 0, for $\lambda > \lambda_c$.

where L is some bulk cut-off that needs to be large enough such that the upper and lower boundaries are fully decoupled, and ϵ is taken to be 10^{-1} . The eigenstates that do not belong to $\text{bulk}(W)$ are assigned to one of the two boundary surfaces which defines the projector $\mathcal{P}_W^{\text{surf}}$

$$\mathcal{P}_W^{\text{surf}}(\vec{x}, \vec{x}') = \left[\delta_{\vec{x}, \vec{x}'} - \sum_{|\psi_n\rangle \in \text{bulk}(W)} \psi_n(\vec{x}')^* \psi_n(\vec{x}) \right] \theta(z - \lfloor N_z/2 \rfloor) \theta(z' - \lfloor N_z/2 \rfloor), \quad (\text{S26})$$

where $\theta(z)$ is the Heaviside theta function, and we assumed that the plane $z = \lfloor N_z/2 \rfloor$ passes through the middle of the slab. As the system approaches metallic phase, portion of surface-localized states decreases to zero, see Fig. 5b.

D. Quantized Hall reponse of TLIs

In this Appendix, we give further details on the measurement setup for the quantized response probing the bulk topology of TLIs using Corbino geometry. As stated in the main text, a non-zero quantized Hall conductance can be measured in genus-one (Corbino) geometry. Below we propose a setup, inspired by the setup of Ref. 54, that shows unique quantized signature of the bulk topology of TLIs.

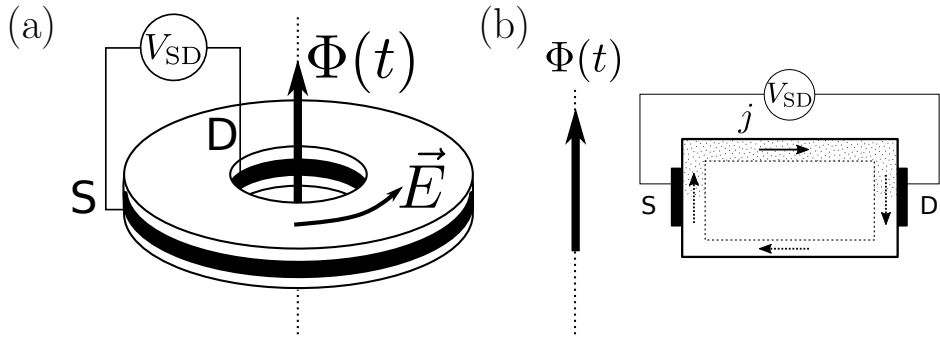


FIG. 6. (a) A non-trivial TLI in Corbino geometry is threaded by magnetic flux $\Phi(t) = \Phi_0 t/T$, with a large source-drain voltage V_{SD} applied. (b) The cross section of the Corbino setup. As the magnetic flux is varied, the charge $\sigma_{12}^0 h/e$ is being pumped via the top surface (Laughlin pump). The dotted region (top surface) is filled with electrons in the steady-state, while the bulk is assumed to be empty.

Consider a thick Corbino disc, as shown in Fig. 6a, and assume that the boundary is doped with electrons, such that *all* boundary states are occupied. In this setup, an extrinsic second-order TI [47], which consists of a trivial

fully-localized bulk with a Chern insulator covering (fully or partially) its boundary, does not react to (adiabatic) time-dependent magnetic flux insertion $\Phi(t) = \Phi_0 t/T$. On the other hand, according to Laughlin argument, the boundary of TLIs pumps $\sigma_{12}^0 h/e^2$ electrons during the period T around its cross-section, see Fig. 6b. In order to measure this charge pumping, a source-drain voltage, much larger than the bulk mobility gap, is applied. In the presence of such voltage, the charge is removed from the bottom surface during the pumping. Hence, we expect that in the steady state the top surface remains fully occupied, while the bottom one is empty, see Fig. 6b. (We neglect the effects of the charging energy.) Although such a non-uniform boundary Fermi energy E_F^0 gives rise to chiral states, these states do not connect source to drain: the quantized transfer of $\sigma_{12}^0 h/e^2$ electrons during one period T occurs via pumping of the boundary states from source to drain via the top surface.

E. Relation between TLIs and N -band Hopf insulators

The models of TLIs, introduced in Eq. (1), as well as its N -band generalization discussed in the main text and App. A, become translationally invariant if we change $W_{\vec{R}\alpha}$ from being random numbers to $W_{\vec{R}\alpha} = \alpha$, with $\alpha = 1, \dots, N$. Such deformation of the model does not change the unitary (S1); The resulting, translationally invariant model, corresponds to topologically non-trivial N -band Hopf insulator [42]. Nevertheless, TLIs and N -band Hopf insulators are distinct phases of matter: the constraint of fully-localized bulk implies that TLIs are insulating at an arbitrary filling, whereas N -band Hopf insulators are insulating at integer fillings while being conducting at fractional fillings. This distinction is important, since it implies that the boundary Fermi energy E_F^0 of N -band Hopf cannot be varied independently of that of the bulk. As a consequence, its quantized boundary response can be measured only in a transient state [42].

Topology of N -band Hopf insulator crucially depends on the presence of translational symmetry. For example, inclusion of perturbations that reduce the translational symmetry down to one of its subgroups can trivialize N -band Hopf insulators [42]. Nevertheless, we show that every N -band Hopf insulator can be deformed to a TLI phase with the same bulk topological invariant. We illustrate this point using $N = 2$ Moore-Ran-Wen model [43]. The two-band Bloch Hamiltonian is defined as

$$h_{k_x k_y k_z} = \vec{v} \cdot \vec{\sigma}, \quad (\text{S27})$$

with $v_i = \vec{z}^\dagger \sigma_i \vec{z}$, where $\vec{z} = (z_1, z_2)^T$, with $z_1 = \sin(k_x) + i \sin(k_y)$ and $z_2 = \sin(k_z) + i[\cos(k_x) + \cos(k_y) + \cos(k_z) - \frac{3}{2}]$. The unitary $U_{\vec{k}}$, that diagonalizes above Bloch Hamiltonian, has a non-zero third winding number $\nu[U_{\vec{k}}] = 1$. The two normalized eigenvectors of the Bloch Hamiltonian (S27) are

$$\begin{aligned} |u_{\vec{k}1}\rangle &= |\vec{z}\rangle^{-1} (z_1, z_2)^T, \\ |u_{\vec{k}2}\rangle &= |\vec{z}\rangle^{-1} (z_2^*, -z_1^*)^T, \end{aligned} \quad (\text{S28})$$

which are continuous functions of \vec{k} . We extend these two Bloch eigenvectors to the whole lattice by defining $\psi_{\vec{k}\alpha}(\vec{x}) = e^{-i\vec{k}\cdot\vec{x}} u_{\vec{k}\alpha}(\vec{x})$. Using these two Bloch eigenvector, we define Wannier functions $|w_{(0,0,0)\alpha}\rangle$, $\alpha = 1, 2$,

$$|w_{\vec{R}\alpha}\rangle = \frac{1}{\sqrt{N_x N_y N_z}} \sum_{\vec{k}} e^{i\vec{k}\cdot\vec{R}} |\psi_{\vec{k}\alpha}\rangle. \quad (\text{S29})$$

We use the above Wannier functions to define the following disordered Hamiltonian

$$H_1 = \sum_{\vec{R}\alpha} W_{\vec{R}\alpha} |w_{\vec{R}\alpha}\rangle \langle w_{\vec{R}\alpha}|. \quad (\text{S30})$$

As the bulk Wannier functions of the Hopf insulator are exponentially localized, the unitary $U |w_{\vec{R}\alpha}\rangle = |w_{\vec{R}\alpha}\rangle$ satisfies localization condition (4) and the winding number can be computed using (S10), $\nu[U] = \nu[U_{\vec{k}}] = 1$. By virtue of the bulk-boundary correspondence of the Hopf insulator [42, 44], imposing open boundary conditions in any of the three spatial directions results in surface Chern number equal to $\nu[U] = 1$.